AMS Home Journals Home Journal Archive Subscribe For Authors Help Advanced Search Search [Go]

Full Text View

Radiation of Energy from Nonzonal Ocean Currents, Nonlinear Regime. Part II: Interactions between Waves*

Igor V. Kamenkovich[+]

MIT/WHOI Joint Program, Woods Hole Oceanographic Institution, Woods Hole, Massachusetts

Joseph Pedlosky

Department of Physical Oceanography, Woods Hole Oceanographic Institution Woods Hole, Massachusetts

ABSTRACT

This article continues the study of the radiation of energy from nonzonal ocean currents in the nonlinear regime. The effects of the interactions between different waves in the initial spectrum on the radiating properties in the model are studied. The process is modeled by three numerical experiments, each initialized with a pair of waves. One wave is typically less radiative than the other.

The development of radiation by an initially nonradiating set of modes is observed. The radiative response in the far field is dominated by the waves with a spatial scale longer than the jet width. A brief comparison of the results to the data in the North Atlantic is presented at the end.

Options:
- Create Reference
- Email this Article
- Add to MyArchive
- Search AMS Glossary

Search CrossRef for:
- Articles Citing This Article

Search Google Scholar for:
- Igor V. Kamenkovich
- Joseph Pedlosky

1. Introduction

The possibility to describe the eddy variability in the interior of the North Atlantic as being in large part remotely induced by the Gulf Stream represents an intriguing problem. Several preceding studies have addressed this issue and modeled the process of energy radiation from the Gulf Stream as the radiation of Rossby waves from a time-dependent solid boundary that is zonally oriented (Flierl and Kamenkovich 1975; Pedlosky 1977; Hogg 1988; Malanotte-Rizzoli et al. 1995, etc.). In a second group of studies, the unstable modes of a thin oceanic jet are tested for their ability to radiate energy (Talley 1983;

Kamenkovich and Pedlosky 1996).

In Kamenkovich and Pedlosky (1996), we present a simple model of a *nonzonal* oceanic current. The results show that the horizontal tilt of the jet axis allows slowly growing linear solutions to be radiating. These waves correspond to the parameters near a long-wave stability cutoff of the dispersion curve for each unstable mode. Other solutions are strongly trapped to the mean current. Their fast exponential growth is believed to be the main reason for their spatial trapping; for details see Kamenkovich and Pedlosky (1996).

In Part I of the present study (Kamenkovich and Pedlosky 1998, hereafter Part I), we have considered the nonlinear development of a single linear mode of a nonzonal jet. Those solutions that are trapped during the linear stage of development now become radiating when their fast growth slows due to the nonlinear effects. Although the results provide us with important information about the nonlinear evolution of the radiating linear solutions, the single wave development cannot completely describe the dynamics in the model. More realistic initial conditions should generally contain the whole spectrum of Fourier modes and the nonlinear results can be expected to depend on the particular form of the spectrum.

It is impossible to consider all combinations of initial conditions, but we can greatly simplify the task and study the effects that two initially excited linear modes have on each other. The interactions between those waves will alter the dynamical properties of each of them. Considering those changes, we can deduce important information about the effects of nonlinear interactions between waves in an arbitrary set of linear modes. By doing that, we do not pretend to obtain the complete dynamical picture. Rather, we hope to illustrate with these simple examples the processes going on in the finite-amplitude development of more complicated initial conditions.

In Fig. 1 ⊙═, the linear results for two modes are summarized by presenting the growth rates as functions of x-wavenumber k, where x is the coordinate along the tilted jet's axis. For the experiments, we choose a strongly radiating wave and a wave that is initially faster growing and less radiating; the choices of parameters for this study are shown in the plot. Both waves initially develop independently in agreement with linear theory, but start to influence each other as soon as they reach finite amplitudes. The effects of the development of each primary wave on the radiating behavior of the other one is our main focus here.

We initialize the problem with a sum of two primary linear waves with x-wavenumbers k_1 and k_2. As in the case of single wave, a set of secondary harmonics is generated: components "0," "$k_1 + k_2$," "$k_2 - k_1$," "$2k_1$," "$2k_2$," and so forth. Both primary modes can directly influence each other through these harmonics if $2k_1 = k_2$, in which case the interactions are the strongest. Two waves can also interact indirectly if $2k_1 \neq k_2$; then neither of the secondary harmonics can directly affect primary modes.

The individual evolutions of the waves whose interactions are studied here have been considered in Part I of this study. The comparison of the results between Part I and Part II should help to understand the effects of the joint evolution of linear waves on their individual radiating properties.

The numerical model and the method of analysis remains the same as in Part I. For all computations, the jet axis makes an angle of 30° with respect to the latitude circles. The nondimensional planetary vorticity gradient $\beta^* L^2_{jet}/U$ is 1 (where L_{jet} is the jet half-width and U is its maximum speed).

We will also keep the same notations for 1) the Fourier coefficients $\Psi_{k_n}(y, t)$ of the Fourier component "k_n"; 2) energy K_{k_n} corresponding to this component; and 3) the external part of energy E_{k_n}, integrated from $-\infty$ to -2 and from 2 to $+\infty$. The reader is referred to Part I for the complete description. Three cases, case 1, case 2, and case 3 are considered in sections 2, 3, and 4 correspondingly. The comparison of results with observations from the North Atlantic is presented in section 5.

2. Case 1: Direct interactions

In this numerical experiment we consider the sum of mode 1 with $k = 1$ and mode 2 with $k = 2$ as initial conditions. We make the initial amplitude of a latter wave 2.4 times smaller than that of mode 1. If both waves were growing exactly proportionally to $e^{kc_i t}$, mode 2 would be 3 times as large as mode 1 by the time $t = 12$. The nonlinear effects, however, slow the growth of both modes and make them similar in size during the whole development.

Both modes are going to strongly feel the presence of each other. Indeed, the secondary harmonic produced by self-interactions of mode 1 has an x wavenumber that equals 2; at the same time mode 1 interacts with mode 2 and creates a

harmonic with $k = 1$. Both the harmonics add to the primary modes and can significantly change the energy partition between different wavelengths.

As we recall from Part I, the secondary harmonic of nearly antisymmetric mode 1 is antisymmetric as well. In contrast, mode 2 with $k = 2$ is almost symmetric and this difference in structure makes it possible to determine how strongly mode 2 is modified by the secondary harmonic of mode 1.

We first present the 2D contour plots of the total streamfunction $\Psi(y) + \Psi(x, y, t)$ (Fig. 2 ⊙). The solution remains trapped until $t = 24$ when radiation in the x-independent form starts for negative y. Individual eddies are formed later in both the external regions. The dominant x wavenumber of these eddies is $k = 1$ since two identical eddies are observed in the x direction, and $2 \times 2\pi/L_x = 1$, where L_x is the width of the numerical domain in the x direction. The eddies are elongated in the east–west direction to the north of the jet axis and are nearly parallel to the jet axis to the south from the jet.

To study the structure of the solution in greater detail, we now consider the plots of Fourier coefficients Φ_0, Φ_1, and Φ_2 shown in Fig. 3 ⊙. Component "0" follows a familiar path of development seen in Part I and radiates first for negative y and then for the rest of the domain. The amplitudes of the radiating response are large because the self-interactions of a primary component "1" produce a significant portion of the x-independent component of the streamfunction, which radiates efficiently.

The evolution of x-dependent components "1" and "2" deserves further attention. Initially, components "1" and "2" are easily recognized as almost antisymmetric mode 1 and symmetric mode 2. Both the components are significantly modified later by nonlinear interactions with each other (see, e.g., $t = 44$).

As we remarked before, it is useful to compare the results of this section with the individual evolution of either of modes. We begin with component "1" and see that the radiation now starts much earlier than in the case with single mode 1, in which case it starts at $t = 48$ as we saw in Part I. That is attributed to the fact that now mode 1 is given 5 times larger initial amplitude. The radiation in the model typically starts at the beginning of nonlinear equilibration following the stage of the rapid exponential growth; the equilibration begins earlier if initial amplitude is larger.

During the late stage of development, the amplitude of component "1" is small. In addition, we see in the energy plots (Fig. 4a ⊙) that energy of component "2" K_2 becomes larger than that of component "1" K_1 after $t = 32$ and K_1 further decreases at later times. It is also interesting to note that component "2" remains nearly symmetric in the immediate vicinity of the jet, which points to the weak contribution of nearly antisymmetric secondary harmonic of mode 1. We can conclude that the jet region is dominated by mode 2 during the advanced stage of nonlinear development.

In contrast, component "1" clearly dominates over component "2" in the exterior starting from $t = 32$ (see also Fig. 2 ⊙). As a result, component "1" radiates as much as almost 15% of K_e by the end of the numerical experiment. The ratio E_1/K_e between external energy of component "1" and total perturbation energy is therefore very close to that for the case with a single mode 1; see Fig. 4 ⊙.

The radiation by component "2" starts much later than in the case with a single mode 2 with $k = 1.8$ ($t = 52$ compared to $t = 24$ for a single mode; see Part I). The beginning of radiation is delayed by development of the radiating response by component "1." The radiation is also weaker than that by component "1." Component "2" slowly extends into both the external regions, which are dominated by the longer and more radiating component "1."

Nevertheless, as much as 11% of K_e is transferred by component "2" into the external regions (Fig. 4b ⊙). The number is twice as large as $E_{1.8}/K_e$ reported in section 5e. The difference can be explained by the contribution of the secondary harmonic "2" produced by self-interactions of the radiating component "1" in case 1. The value of E_2/K_e is also twice as big as the same quantity in the case with a single mode 1 in which mode 2 with $k = 2$ is excited only on the late stage of development.

The joint radiation by all components is very effective: $(E_0 + E_1 + E_2)/K_e$ is more than 35%. The value of the ratio is close to the same quantity in the case of a single mode 1 (section 6 of Part I).

3. Case 2: Indirect interactions

We have observed in the previous section that the weakly radiating mode 2 eventually dominates the nonlinear development in the jet region but does not prevent mode 1 from radiation. Rather, component "1" prevails in the exterior

regions; it produces a second harmonic with $k = 2$ that increases the radiation by component "2." What changes if direct mutual feedback between two primary modes is not possible?

To answer this question, we carry out a numerical experiment in which we initialize the model with mode 1 with $k = 1$ and mode 2 with $k = 1.5$. The self-interactions of mode 1 produce component "2" as before but now it does not directly affect mode 2. The nonlinear interactions produce secondary harmonics "0.5," "2," "2.5," and "3"; neither of them can influence component "1" directly. It is therefore interesting to compare the results in case 2 with the results in case 1. That will help us to understand the role of interactions between modes in the dynamics of the problem.

As in case 1, mode 1 is given larger initial amplitude than mode 2. If both waves were growing exactly proportionally to $e^{kc_i t}$, mode 2 would be larger than mode 1 by 3 times by the time $t = 14$.

Two-dimensional contour plots of the total streamfunction $\Psi(y) + \psi(x, y)$ (Fig. 5 ⊙) provide us with general information about the structure of the solution. As in case 1 (Fig. 2 ⊙), the solution is asymmetric in the y direction. Eddies to the north from the jet are oriented east–west, whereas eddies to the south ($y < 0$) are elongated in the direction of the jet axis. The differences between case 1 and case 2 are also obvious to a viewer. The dominant scale in the x direction is now twice as large as in case 1, which indicates the dominance of the component with $k = 0.5$ wavenumber (since $2\pi/L_x = 0.5$). The trapped meanders seem to be a mixture of two components with wavenumbers $k = 1$ and $k = 0.5$.

The Fourier coefficients are shown in Fig. 6 ⊙. As in case 1, component "0" starts its radiation for negative y after $t = 20$. The amplitude of its radiating part reaches large amplitudes at later times. We now focus on the differences in the development between components "1" and "1.5" in case 2 and components "1" and "2" in case 1.

Component "1" in case 2 has larger amplitudes than in case 1, especially during the late stage of development ($t > 32$) as can be seen in Fig. 6 ⊙. The difference is striking at $t = 52$. In contrast, component "1.5" remains small until $t = 36$. As in case 1, it then slowly overcomes component "1" in terms of the amplitude in the jet region ($t = 36$). Component "1.5" then starts to slowly expand into both the external regions. The switch in the relative importance between two components is clearly seen in Fig. 7a ⊙ where the corresponding kinetic energies are presented. Shortly after $t = 40$, $K_{1.5}$ becomes larger than K_1.

It is also interesting to observe the rapid growth of component "0.5" (Fig. 6 ⊙ and Fig. 8 ⊙, upper panel; see also the discussion of Fig. 5 ⊙ above). The component is produced by the interactions between two primary components "1" and "1.5." Its energy $K_{0.5}$ becomes larger than the energy of any other secondary components in the plot at the same time as component "1.5" begins to dominate in the development ($t > 40$; upper panels of Figs. 7 ⊙ and 8 ⊙). Simultaneously, the energy of component "2," which is the result of self-interactions of component "1," decreases together with K_1 (Fig. 8 ⊙, upper panel). Here $K_{0.5}$ is an order of magnitude larger than $K_{2.5}$, which is another secondary harmonic produced by the interactions between two primary modes. The longest of two secondary harmonics is clearly more energetic.

One interesting and somewhat puzzling fact is the high values of a perturbation energy corresponding to each of the components. Both K_1 and $K_{1.5}$ are much larger than K_1 and K_2 in case 1. In an experiment not presented here, the problem was initialized with a single mode 1 with the same amplitude as in case 1 and case 2. The resulting K_1 was as large as in the case 2; small K_1 in case 1 can be explained by the direct suppression by the mode 2. Secondary components further contribute to the total value of the perturbation kinetic energy; see Fig. 8a ⊙. As a result, the value of K_e is much larger than in case 1.

The absence of direct interactions with component "1" has a dual effect on the radiating properties of component "1.5." The latter is no longer directly suppressed by the vigorously radiating component "1" in the external regions. In fact, $E_{1.5}$ becomes larger than E_1 at the same time as the total energy of this component $K_{1.5}$ becomes the largest as well (Fig. 7b ⊙). On the other hand, secondary harmonic of component "1" cannot put the external energy into component "1.5" as in case 1.

As a result, $E_{1.5}/K_e$ is almost the same as E_2/K_e in case 1 by the end of development. Presumably, the absence of both the suppression and the feedback by the component "1" compensate each other and result in little overall effect on the effectiveness of radiation by component "1.5."

In contrast, the effectiveness of the radiation by component "1" is less in case 2 than in case 1; compare 8% in Fig. 7b ⊙ to almost 16% in Fig. 4b ⊙. In case 1, the presence of direct mutual feedback between two primary modes enables the

long and more radiating component "1" to account for the major part of the radiated energy.

In case 2, the energy instead escapes into radiating secondary harmonics that do not project back onto any of primary modes. In particular, self-interactions of component "1" produce component "2" that develops on its own. One can see in Fig. 8b component "2" is associated with E_2 that is almost 4% of K_e.

As was noted above, the interactions between two primary components "1" and "1.5" produce another very energetic harmonic, component "0.5." The component is also strongly radiating: $E_{0.5}/K_e$ is almost 12%, which is even bigger than E_1/K_e (Fig. 8b). Its large amplitudes in both the external regions are evident in Fig. 6 and in Fig. 5 . Once again we observe that waves that are longer in x are more radiating; in our case, even a secondary component "0.5" can dominate the radiating response in the exterior.

The radiation in case 1 with no direct mutual feedback between two primary components is more energetic than in case 1 with direct interactions. The ratio of the sum of all external energies to the total energy $(E_0 + \ldots + E_3)/K_e$ is more than 39% by $t = 52$, which is slightly bigger than 35% in case 1. We now recall that the value K_e itself is much larger in case 2 (Figs. 4 and 7).

We can conclude that the absence of direct mutual feedback between a strongly radiating wave of mode 1 and a weakly radiating wave of mode 2 allows the development of strongly radiating secondary harmonics. The radiating properties of mode 2 appear almost to be not affected.

4. Case 3: Mode 1

The study of interactions between different types of linear solutions would be incomplete without the experiment in which the development of a long and a short wave of mode 1 is considered. For the experiment we choose $k = 0.25$ and $k = 1$ as corresponding wavenumbers. The amplitude of the longest wave of the pair is 4 times larger than the amplitude of the wave with $k = 1$.

As we recall from Part I, both waves are strongly radiating in the nonlinear regime. The wave with $k = 1$ has a growth rate almost twice as large as that of a wave with $k = 0.25$. Therefore, the former has a tendency to dominate in the development. On the other hand, a wave with $k = 0.25$ is more radiating. Which of the two waves will dominate the development in the exterior regions?

The direct mutual feedback between two waves is not possible for our choice of parameters. The situation is similar to case 2, described above, in which neither of secondary harmonics created in the course of nonlinear development can directly affect the primary modes. However, some differences should be anticipated. First, the shortest primary wave with $k = 1$ is capable of significant radiation, unlike mode 2 for $k = 1.5$ in case 2. Second, both secondary harmonics "0.75" and "1.25" produced by the interactions between primary modes are shorter than the longest primary wave with $k = 0.25$. In contrast, one of the secondary harmonics in case 2, namely component "0.5," is the longest in a set and dominates the radiative response in the far field. Which component is the most energetically significant in the far field in case 3?

To answer these questions, we first present the 2D contour plots of the total streamfunction $\Psi(y) + \psi(x, y)$ in Fig. 9 . The evolution of the structure of the solution is very different from case 1 and case 2 (Figs. 2 and 5). The radiation starts as early as $t = 32$ and is in the form of isolated eddies of various forms, unlike either of case 1 or case 2 in which the radiating response is x independent initially.

By the end of numerical experiment at $t = 64$, the radiated eddies fill the entire numerical domain, which is 50 times as large as the width of the jet itself. The orientation of these eddies is different from that in either of the previous cases described in this chapter. In fact, eddies are elongated in a direction nearly perpendicular to the jet axis for $y > 0$. The eddy axes to the south from the jet are tilted relative to both the jet axis and latitude circles. The complicated structure of the solution indicates the importance of several x wavenumbers.

We now proceed with the detailed analysis of the structure of the solution and show the Fourier coefficients in Fig. 10 . In the way similar to a single mode 1 development in Part I, the radiation of the component "1" starts at $t = 40$ immediately following the radiation by component "0." The exterior part of component "1" later reaches amplitudes as large as in the case with a single mode 1 [section 5d(1)]. The development of component "1" seems to be very little affected by the presence of the long component "0.25," which does not directly influence the former.

In contrast, component "0.25" develops differently in case 3 compared to the case with a single mode 1 for $k = 0.25$ (see Part I). Although component "1" does not directly influence component "0.25," a smaller portion of the total energy is

available for the development of the latter because of the rapid growth of component "1." As a result, the amplitude of the component is smaller in case 3 than in the case with a single mode for $t > 40$.

Another very interesting property of the development in case 3 is the very energetic component "1.25" that is a harmonic created by the nonlinear interactions between two primary modes. The amplitude of this component becomes larger than the amplitudes of both the primary modes by $t = 64$ in the jet region. The harmonic also has a well-pronounced symmetric component there, which suggests the possible excitation of mode 2 with $k = 1.25$. As discussed above and in Part I, the nonlinear interactions of nearly antisymmetric mode 1 create harmonics that are in turn almost antisymmetric.

We now consider the values of E_{k_n}/K_e plotted in Fig. 11 . Component "0.25" is weakly trapped initially, which is reflected in the high values of $E_{0.25}/K_e$ at the beginning of the numerical experiment: 11% at $t = 8$. It then starts to decrease, indicating the rapidly growing importance of other components in the external regions. The decrease is especially sharp after $t = 24$;$E_{0.25}/K_e$ is only 3% during the second half of the experiment. The contribution of component "0.25" to the energy in the exterior regions is rather small, especially if compared with 18% in the case of a single mode in Part I.

Simultaneously with the decline of the importance of component "0.25" in the external regions, E_1/K_e rapidly increases. The ratio reaches 11% by $t = 64$. As we observed in Fig. 10 , the second primary component "1" is of approximately the same amplitude as component "0.25." The latter, however, is not suppressed by component "1"; its amplitude remains large (Fig. 10). Nevertheless, since component "1" is shorter in x, it corresponds to larger kinetic energy than a longer primary component "0.25."

The values of E_{k_n}/K_e for secondary harmonics plotted in Fig. 11b are very interesting. In particular, component "1.25," which is created by the interactions between two primary components "0.25" and "1," corresponds to the value of the external kinetic energy that is as large as $E_{0.25}$; $E_{1.25}$ is more than 11% of K_e. The same component is also very energetic in the case with a single component "0.25" in Part I.

Other secondary harmonics radiate less than 4% of the total energy K_e each. However, the radiation in case 3 is very efficient. Altogether, all components radiate almost 45% of the total kinetic energy into both the external regions. This number is higher than the same quantity in the case with a single wave for $k = 1$ but lower than in the case with a wave for $k = 0.25$ in Part I.

We can conclude that although component "0.25" radiates very efficiently when the problem is initialized with a single wavenumber $k = 0.25$[section 5d(2)], it does not dominate the radiating response in case 3. Shorter waves, which correspond to more realistic spatial scales, have amplitudes at least as large as those of component "0.25." Moreover, the major part of radiated energy corresponds to those shorter scales in case 3.

5. Comparison with observations in the North Atlantic

We have formulated and solved the problem of stability of a nonzonal ocean current. The focus of the research was on the ability of unstable perturbations to effectively transfer energy from an energetic mean current into the far field. By doing that, we attempt to model the Gulf Stream as an energy source for the eddy field in the interior of the North Atlantic gyre. How relevant are our results to the real phenomena observed in the region?

To answer this question, we need to compare the model predictions to the observations in the North Atlantic. In doing the comparison, we hope to understand to what degree the complicated dynamical process of the generation of highly energetic eddy fields can be explained by the radiation of energy from the Gulf Stream described by our model.

We cannot claim that our simple model is an accurate representation of the Gulf Stream system and instead we are more interested in its ability to capture general dynamic properties in the region.

a. Scaling of results

The comparison of our simple barotropic model to the real Gulf Stream is not easy because of the simplified vertical and horizontal structure of the mean current in the model. We base our scaling on keeping such physical quantities as the total transport, the width, and maximum velocity of the current as close as possible to being realistic.

The data for the Gulf Stream are taken from Johns et al. (1995), in which the authors report the structure and transport of the current near 68°W using SYNOP current meter observations. Velocities are considered in the rotated, downstream

coordinate frame.

Two parameters are needed for scaling: the half-width of the jet L_{jet}, which is defined as a distance from the point of maximum velocity to the point of zero velocity, and the maximum jet velocity U. We choose the first value to be 125 km based on the vertical profile of the velocity of the current given in Johns et al. (1995).

The next parameter to be estimated from observations is the maximum velocity of the barotropic jet in the model. The difficulty is that the Gulf Stream velocity changes in the vertical and its maximum value at each depth varies from almost 2 m s^{-1} at depth 50 m to 0.12 m s^{-1} at the depth of 2 m. For the value of U, we choose to average these peak values over the depth of 2 km, which gives us approximately $U = 0.5$ m s^{-1}.

Before we proceed any further, we need to check if the volume transport in the model is reasonably close to the observed value. The dimensional transport per unit depth can be computed in the model to yield approximately 56 Sv/km. We now take the number for the total transport at 68°W from the surface to 2 km from Table 1 in Johns et al. (1995) and divide the obtained 99 Sv by the water column depth. We get 50 Sv/km, which is very close to the corresponding value in the model. Our choice of dimensional parameters is consistent with the observed value of the volume transport.

We also should note that for the parameters chosen, the value of nondimensional planetary vorticity gradient $\beta = \beta$ $*L^2_{jet}/U$ is approximately 0.6. This value is in between two choices for this parameter, namely 1 and 0.25, in the experiments used for the comparison below.

b. Perturbation kinetic energy

We choose to analyze the perturbation kinetic energy (PKE) distribution predicted by the model for the brief comparison with observations. The main purpose is to understand to what degree our simple model of energy radiation from the Gulf Stream describes the eddy kinetic energy (EKE) distribution observed in the North Atlantic.

As we have seen in the preceding sections, the details of the results depend on the initial conditions in each experiment. Therefore, a valid comparison should focus on the features that are common in several numerical experiments with very different initial conditions.

We will analyze the model results for four cases with different initial conditions and values of nondimensional $\beta = \beta$ $*L^2_{jet}/U$ ($\beta*$ is the dimensional planetary vorticity gradient): 1) mode 1, $\beta = 1$, $k = 1$ (MR1); 2) mode 1, $\beta = 0.25$, $k = 1$ (MR2); 3) case 2 from this article (MR3); and 4) case 3 from this article (MR4). For all cases, $\alpha = 30°$. The analysis is performed on the advanced stage of nonlinear development during the nonlinear equilibration in the model. We will use the above notations in parentheses for brevity to identify each case. Note that in cases MR1 and MR2 the single wave development is considered.

In the next four contour plots (Figs. 12–15), we present the results from our model for all four cases (MR1–MR4). First thing to notice in all four plots is the high values of PKE centered in the jet region. The band of high energy (values exceeding 500 cm^2 s^{-2}) stretches for more than 500 km in the cross-stream direction for MR2 and MR3. The high-energy band is narrower for MR1 and MR4. The maximum values of PKE reach 1500 cm^2 s^{-2} in the model for MR1, MR2, and MR3. Only in MR4 are areas found in which PKE reaches 3000 cm^2 s^{-2}.

The values of PKE decrease away from the jet region. Values of 200 cm^2 s^{-2} are produced by the model at the distances of approximately 500 km both to the north and to the south from the stream axis in all four cases analyzed. The PKE penetration scale is slightly longer to the south for MR2.

Here, we use the article by Richardson (1983) as a source of data for the comparison. In the article, the author used the velocities of the near-surface currents in the North Atlantic measured by the satellite-tracked drifting buoys to construct kinetic energy maps. The resulting values of the eddy kinetic energy in the Gulf Stream region are two times as high as those obtained from the ship drift measurements (Wyrtki et al. 1976). The results from Richardson (1983) are reproduced in Figs. 16 and 18 .

The observed EKE (Fig. 16) is generally higher than the PKE in the model. The peak values as high as 3000 cm^2 s^{-2} are observed in the Gulf Stream region and are twice as high as the corresponding peak values produced by the model.

The band of high observed EKE with values of more than 1000 cm^2 s^{-2} is centered in the Gulf Stream axis and has a width of approximately 500 km after the current leaves the coast and then broadens to almost 1000-km width (Fig. 16 ⬤▬). If we accept the factor of 2 as the overall difference between the observed values of EKE and the barotropic PKE produced by the model, we can conclude that the meridional scale of the high energy region is reproduced correctly by the model.

There are a number of reasons that might account for the difference between the observed values of EKE and the model results apart from the simplicity of the model. First, the data describe near-surface values of EKE, whereas the eddy field in our barotropic model is depth independent. The observed EKE in the vicinity of the Gulf Stream significantly decreases with depth; for example, the EKE decreases by more than 15 times from the depth of 400 m to the depth of 2000 m at 68°W in the vicinity of the Gulf Stream axis (Schmitz and Luyten 1991). The difference is lower in the regions away from the stream. It is therefore not surprising to find the values of depth-averaged kinetic energy to be smaller than those observed at the surface.

Another reason is associated with the difficulty of choosing the correct initial conditions for our simple model as it was noted above. The level of the PKE produced by a numerical run depends on the amount of the initial kinetic energy. We can compare, for example, MR1 and MR3. In the latter case, mode 2 is added in addition to a single mode 1 of MR1. As a result, MR3 corresponds to higher values of PKE than does MR1. We therefore need to reiterate that we are looking for features common to all four cases (MR1–MR4) that have very different initial conditions, and it is unrealistic to make a detailed comparison to data in each case.

The downstream dependence of the mean current is neglected in the model. As a result, we cannot expect the model to reproduce the observed downstream increase of the EKE related to the increased meander activity. We now concentrate on the cross-stream dependence and look at the distance at which PKE penetrates into the regions away from the Gulf Stream axis. In doing that, we need to keep in mind that the penetration scale increases with time as the perturbations spread in the cross-stream direction due to radiation. The penetration distance at the end of each numerical experiment, therefore, tells us that the significant portion of PKE has gotten *at least this far* from the jet axis. The quantity serves as an important measure of the effectiveness of radiation in explaining the observed broad bands of EKE in the North Atlantic.

Our numerical solution is a sum of a number of waves that results in several isolated maxima of PKE. As a result, the decay scale of the PKE in the meridional direction is difficult to estimate from the 2D contour plots. Instead, we choose to analyze the profile of the downstream-averaged energy (Fig. 17 ⬤▬) and estimate the decay scale in the cross-stream direction.

All four cases (MR1–MR4) are shown in the figure. As one can observe in the plot, MR2 and MR3 correspond to larger values of the averaged kinetic energy than do MR1 and MR4. Note also that the maximum x-averaged values are smaller than the absolute maximum values in the 2D plot due to the strong x dependence of the PKE.

The approximate distance in the direction perpendicular to the jet axis over which the x-averaged PKE e-folds is then computed for each case. The logarithm of the PKE divided by the maximum value of PKE is plotted in the lower panel. One should keep in mind that the jet axis is tilted in the model and the cross-jet direction does not coincide with lines of longitude. As one can see, the e-folding scales are 350 km for MR1 and MR2, 300 km for MR3, and 200 km for MR4 to the south from the jet; 400 km for MR2, 300 km for MR1 and MR3, and 250 km for MR4 to the north from the jet. The decay scale to the south from the jet axis ($y < 0$) is longer than to the north ($y > 0$) for MR1 and MR2; the distribution of x-averaged PKE is more symmetric for MR3 and MR4.

The distribution of the observed EKE shows good agreement with the model results in terms of the spatial decay scales in the cross-jet direction. For example, at 65°W the energy reaches e-folding at 300 km from the axis (as is claimed in Richardson 1983) and is larger to the south and less than to the north (see Fig. 18 ⬤▬). The less rapid decay in the EKE to the south from the stream axis is reproduced by the model results MR1 and MR2.

We stress here that in our simple model, we report the PKE distribution for the nonequilibrated, transient state. A number of physical processes missing in the model is needed for obtaining equilibrated energy field more suitable for direct comparison with data. In particular, we can single out missing dissipation and the absence of the mean flow in the far field in the model. Nevertheless, the above comparison demonstrates the ability of the radiative mechanism to transfer energy over distances corresponding to those observed. Once radiated, this energy represents a source for the eddy field in the interior of the ocean. We find this result encouraging.

6. Summary and conclusions

We have considered three types of interactions between different waves that take place in the nonlinear development of a set of initially linear waves. All types are modeled by the numerical experiments in which the evolution of a pair of linear waves is studied.

As case 1 shows, the direct mutual feedback between a radiating wave of mode 1 and a twice as short weakly radiating wave of mode 2 does not affect the strong radiating ability of the former. Mode 1 still dominates the radiating motions in the far field and the radiation is very effective. However, mode 1 is suppressed by mode 2 in the jet region and its amplitude becomes smaller than in the case with a single mode 1. The case models the "direct" interactions between those waves for which wavenumbers are such to allow secondary harmonics to immediately add to the primary waves. This important result implies that modes of secondary importance within the jet can nevertheless dominate the far-field radiation.

In case 2, direct mutual feedback between two primary waves is not possible because of the values of their wavenumbers. Instead, very energetic secondary harmonics develop. One of those harmonics is the longest wave in the created set; it is also the most radiating component in the experiment. The total perturbation energy is much larger than in case 1.

Unlike case 1, case 2 models the "indirect" interactions between a strongly radiating wave of mode 1 and a weakly radiating short wave of mode 2. Such interactions produce secondary harmonics that do not immediately add to any of primary harmonics. The spectrum broadens as a result. Those harmonics that are long in x are capable of radiation that is more energetic than the radiation by a primary wave alone. The latter fact illustrates the possibility of a cascade of radiating energy into the longer x wavelengths.

In both case 1 and case 2, the radiating field is asymmetric in the cross-jet direction. In the northern half-plane, the eddies are elongated in the east–west direction, whereas the eddies are parallel to the jet axis to the south from the jet.

The mutual development of two strongly radiating waves of mode 1 is considered in case 3. One of the waves is four times longer than the other and radiates more energetically if considered alone. However, in case 3 both short and long waves have similar amplitudes in the exterior regions. The short wave together with its secondary harmonics are associated with the major part of radiated energy. Case 3 models the indirect interactions between strongly radiating waves in a set.

We can draw the main conclusion that energy radiation is not only a feature of the single wave development, but is also present in the evolution of a set of initially nonradiating waves. The general dynamical picture of a development of an initially white spectrum of linear modes is, of course, more complex. However, we have observed the general tendency of a spectrum of kinetic energy in the far field to develop a maximum at $k \sim 1$, which, we emphasize, is not the most unstable mode of the jet. In other words, one should expect the short waves with x-wavenumber $k \sim 1$ to be energetically important in the nonlinear development of any broad spectrum of initial conditions.

An attempt to compare the results of our simple model to the observations in the North Atlantic is then made. In doing the comparison, we emphasize the limitations of the model and its inability to reproduce the observed dynamical fields in detail. However, several general dynamic features of the observed eddy kinetic energy distribution in the North Atlantic are captured by the model moderately well.

The level of PKE in the model appears to be close to the observed one despite the limitations of our simple model. The spatial decay scale achieved in the model by the end of integration time in all cases compares well with the observed values. The model prediction of 300 km for the e-folding scale is supported by observations. The fact demonstrates the ability of the model to reproduce bands of high values of surface EKE that are at least as wide as those observed in the North Atlantic. These results stress the possibility that eddy variability in the North Atlantic interior is in large part remotely generated by the Gulf Stream.

Parts I and II of this work emphasize the importance of the energy radiation from boundary currents as one of the main mechanisms for the generation of eddies in the oceanic interior. As is demonstrated by the results, taking into account such dynamical features of the structure of radiating basic states as their nonzonal orientation can enhance the mechanism.

Further elaboration of the models with radiating basic states should include more realistic downstream dependence of the basic current. The need for the forcing to maintain the mean flow would be eliminated. In addition, periodic boundary conditions in the along-jet direction in our model exclude convective instabilities that may be important in the complete dynamical picture. Open boundary conditions would be required in that case.

The presence of the coast can be another important element in the process. The radiated waves can be reflected and strongly modified as a result. In our model, we had in mind the portion of the Gulf Stream that does not flow along the coast. Since no downflow dependence in the mean current was assumed, it would be difficult to model coastal reflection in our case. The consideration of more realistic geometry and topography is indispensable in future studies.

Making the Rossby deformation radius finite or considering a vertically stratified mean state can also change the results, quantitatively making them more realistic. However, based on the previous linear results (Kamenkovich and Pedlosky 1996),

we can expect the radiation to remain a robust feature of a nonzonal oceanic current with some vertical structure.

Two main results of the present research provide some guidance for the interpretation of ocean general circulation models. First, the correct representation of the nonzonal orientation of the Gulf Stream leaving the coast is apparently crucial for the reproduction of the large-scale distribution of eddy kinetic energy in the North Atlantic. Second, the importance of the nonlocal mechanism for the eddy generation calls into question some existing techniques for the eddy parameterization in terms of the local mean field.

REFERENCES

Flierl, G. R., and V. M. Kamenkovich, 1975: Gulf Stream meandering and Gulf Stream Ring eddy production mechanisms. *Dynamics and the Analysis of MODE-1,* A. R. Robinson, Ed., The MIT Press, 115–118..

Hogg, N. G., 1988: Stochastic wave radiation by the Gulf Stream. *J. Phys. Oceanogr.,* **18,** 1687–1701..

Johns, W. E., T. J. Shay, J. M. Bane, and D. R. Watts, 1995: Gulf Stream structure, transport, and recirculation near 68° W. *J. Geophys. Res.,* **100,** 817–838..

Kamenkovich, I., and J. Pedlosky, 1996: Radiating instability of nonzonal ocean currents. *J. Phys. Oceanogr.,* **26,** 622–643..

—— ,and —— ,1998: Radiation of energy from nonzonal ocean currents. Nonlinear regime. Part I: Single wave development. *J. Phys. Oceanogr.,* **28,** 1661–1682..

Malanotte-Rizzoli, P., N. G. Hogg, and R. E. Young, 1995: Stochastic wave radiation by the Gulf Stream: Numerical experiments. *Deep-Sea Res.,* **42,** 389–423..

Pedlosky, J., 1977: On the radiation of meso-scale energy in the mid-ocean. *Deep-Sea Res.,* **24,** 591–600..

Richardson, P. L., 1983: Eddy kinetic energy in the North Atlantic from surface drifters. *J. Geophys. Res.,* **88,** 4355–4367..

Schmitz, W. J., and J. R. Luyten, 1991: Spectral time scales for mid-latitude eddies. *J. Mar. Res.,* **49,** 75–107..

Talley, L. D., 1983: Radiating barotropic instability. *J. Phys. Oceanogr.,* **13,** 972–987..

Wyrtki, K., L. Magaard, and J. Hager, 1976: Eddy energy in the oceans. *J. Geophys. Res.,* **81,** 2641–2646..

Figures
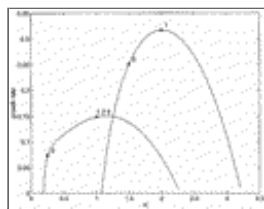
Click on thumbnail for full-sized image.

Fig. 1. Growth rates of linear solutions as functions of x wavenumber k for $\alpha = 30°$ and $\beta = 1$. Mode numbers are given in the plot. The choices of parameters for all experiments are given by stars;the case numbers are given next to corresponding points.
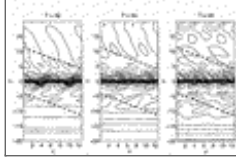
Fig. 2. Two-dimensional contour plots of the total streamfunction $\Psi(y) + \psi(x, y)$. Corresponding times are given on the top of each plot. Heavy dashed lines are parallel to the latitude circles. Case 1: mode 1 ($k = 1$) and mode 2 ($k = 2$); $\alpha = 30°$ and $\beta = 1$.
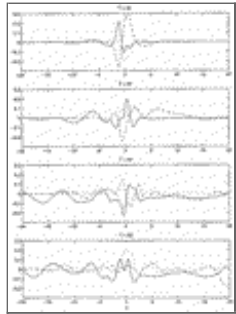
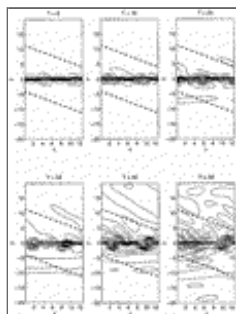Fig. 3. The Fourier coefficients Φ_0 (solid lines), Φ_1 (dashed lines), and Φ_2 (dotted lines) of the streamfunction as functions of y. Corresponding times are given on the top of each panel. Case 1: mode 1 ($k = 1$) and mode 2 ($k = 2$); $\alpha = 30°$ and $\beta = 1$.
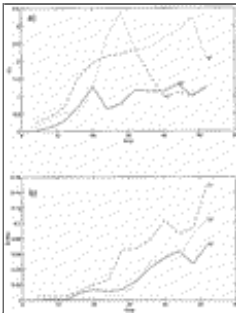
Fig. 4. Kinetic energy corresponding to each Fourier component vs time: (a) K_{k_n} (energy integrated over the whole domain); (b) E_{k_n} (energy integrated from $-\infty$ to -2 and from 2 to ∞) divided by the total energy K_e. Component numbers are shown in the plot. Case 1:mode 1 ($k = 1$) and mode 2 ($k = 2$); $\alpha = 30°$ and $\beta = 1$.

Fig. 5. Two-dimensional contour plots of the total streamfunction $\Psi(y) + \psi(x, y)$. As in Fig. 2 but for case 2: mode 1 ($k = 1$) and mode 2 ($k = 1.5$); $\alpha = 30°$ and $\beta = 1$.
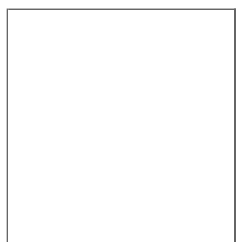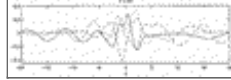
Fig. 6. The Fourier coefficients Φ_0 (solid lines), Φ_1 (dashed lines), $\Phi_{1.5}$ (dotted lines), and $\Phi_{0.5}$ (dashed–dotted lines) of the streamfunction as functions of y. Corresponding times are given on the top of each panel. Case 2: mode 1 ($k = 1$) and mode 2 ($k = 1.5$); $\alpha = 30°$ and $\beta = 1$.
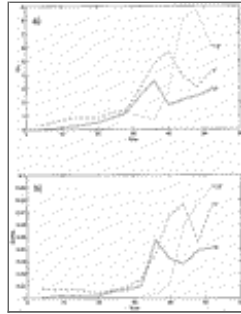
Fig. 7. Kinetic energy corresponding to each Fourier component vs time. As in Fig. 4 but for case 2: mode 1 ($k = 1$) and mode 2 ($k = 1.5$); $\alpha = 30°$ and $\beta = 1$. Components "0," "1," and "1.5." Component numbers are shown in the plot.
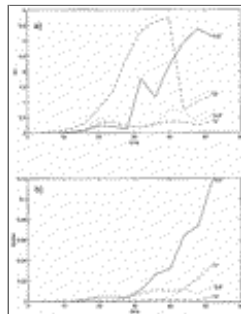
Fig. 8. As in Fig. 4 but for components "0.5," "2," and "2.5."Case 2: mode 1 ($k = 1$) and mode 2 ($k = 1.5$); $\alpha = 30°$ and $\beta = 1$.
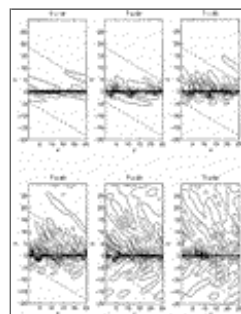
Fig. 9. Two-dimensional contour plots of the total streamfunction $\Psi(y) + \psi(x, y)$. As in Fig. 2 but for case 3: mode 1 with $k = 0.25$ and $k = 1$.
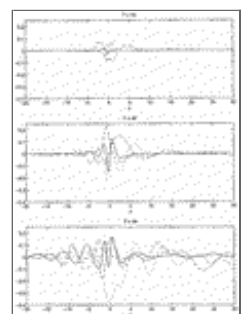
Fig. 10. The Fourier coefficients Φ_0 (solid lines), $\Phi_{0.25}$ (dashed lines), Φ_1 (dashed–dotted lines), and $\Phi_{1.25}$ (dotted lines) of the streamfunction as functions of y. Corresponding times are given on the top of each panel. Case 3: mode 1 for $k = 0.25$ and $k = 1$; $\alpha = 30°$ and $\beta = 1$.
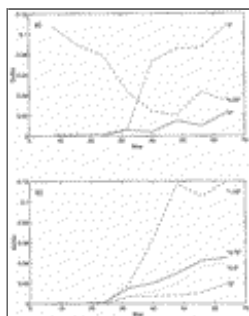
Click on thumbnail for full-sized image.

Fig. 11. External kinetic energy corresponding to each Fourier component, E_{k_n}, divided by the total energy K_e. Case 3: mode 1 for $k = 0.25$ and $k = 1$; $\alpha = 30°$ and $\beta = 1$.
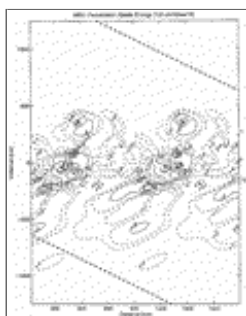
Click on thumbnail for full-sized image.

Fig. 12. PKE for MR1. The dashed contours show low values of the energy (<500 cm^2 s^{-2}). The heavy dashed lines show latitude circles. Units are 100 cm^2 s^{-2}.
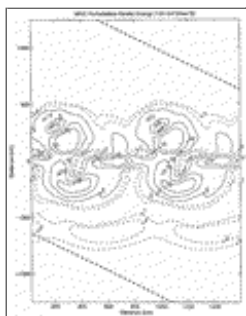
Click on thumbnail for full-sized image.

Fig. 13. As in Fig. 12 but for MR2.
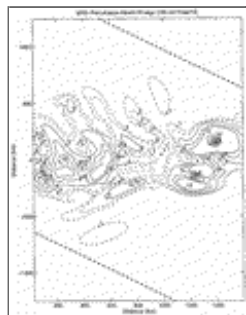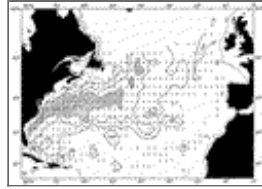

Click on thumbnail for full-sized image.

Fig. 14. As in Fig. 12 but for MR3.
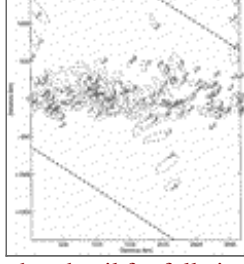
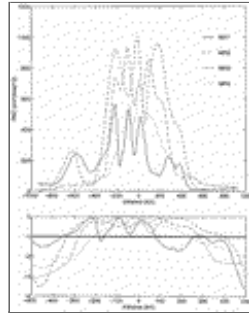Click on thumbnail for full-sized image.

Fig. 15. As in Fig. 12 ⊙ but for MR4.

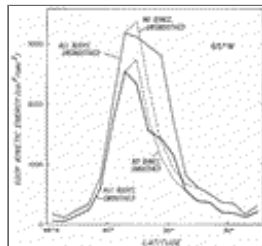Click on thumbnail for full-sized image.

Fig. 16. EKE (cm^2 s^{-2}) in the North Atlantic. After Richardson (1983, Fig. 10 ⊙).

Click on thumbnail for full-sized image.

Fig. 17. Upper panel: PKE averaged in the downstream direction for all four cases. Types of lines corresponding to the each of four cases are given in the plot. The negative values of y correspond to the region to the south from the jet axis. Lower panel: The logarithm of PKE/max(PKE). The thick line shows -1.

Click on thumbnail for full-sized image.

Fig. 18. EKE at 65°W. Different curves show the effect of smoothing the data and excluding ring observations. After Richardson (1983, Fig. 13).

Corresponding author address: Dr. Igor V. Kamenkovich, Massachusetts Institute of Technology, Bldg. E40, Room 263, Cambridge, MA 02139.

E-mail: igor@gyre.mit.edu